Assimilation of All Sky Infrared Radiance from INSAT-3D/3DR Satellite in the WRF Model

Prashant Kumar[1], Munn Vinayak Shukla[1], and Atul K Varma[1]

[1]Indian Space Research Organisation

November 24, 2022

Abstract

The all-sky Infrared (IR) radiance assimilation from geostationary satellites has been a prime research area in the numerical weather prediction (NWP) modeling. In this study, the variational data assimilation system of the weather research and forecasting (WRF) model has been customized to assimilate all-sky assimilation of water vapour (WV) radiance from Imager onboard two geostationary Indian National Satellites (INSAT-3D and INSAT-3DR). This study also integrated different hydrometeors (like cloud, rain, ice, snow and graupel) as control variables in the WRF variation assimilation system. To do this, parallel experiments were performed by carrying out model simulations with and without INSAT WV radiance assimilation during July 2018. Results of these simulations suggested that the WRF model analyses for all-sky assimilation are closer to the brightness temperature (T_B) of channel-1 (183.31 $\pm$ 0.2 GHz) of SAPHIR (Sondeur Atmosphérique du Profil d'Humidité Intertropicale par Radiométrie) sensor onboard Megha-Tropiques satellite and channel-3 (183.31 $\pm$ 1.0 GHz) of MHS (Microwave Humidity Sounder) sensor onboard National Oceanic and Atmospheric Administration (NOAA-18/19) and Meteorological Operational Satellite (MetOp-A/B/C) satellites. Furthermore, noteworthy changes are noticed in hydrometeors analyses with all-sky assimilation and the number of assimilated observations are increased significantly (around 2.5 times). The short-range predictions from all-sky assimilation runs revealed notable positive impact as compared to clear-sky assimilation runs when verified with SAPHIR and MHS T_B, and NCEP (National Centers for Environmental Prediction) final analysis.

Assimilation of All Sky Infrared Radiance from INSAT-3D/3DR Satellite in the WRF Model

Prashant Kumar[1], Munn V. Shukla[2], and A. K. Varma[1]

1. Atmospheric Sciences Division, Atmospheric and Oceanic Sciences Group, EPSA, Space Applications Centre, ISRO, Ahmedabad, India

2. Geo-physical Parameter Retrievals Division, Atmospheric and Oceanic Sciences Group, EPSA, Space Applications Centre, ISRO, Ahmedabad, India

Abstract

The all-sky Infrared (IR) radiance assimilation from geostationary satellites has been a prime research area in the numerical weather prediction (NWP) modeling. In this study, the variational data assimilation system of the weather research and forecasting (WRF) model has been customized to assimilate all-sky assimilation of water vapour (WV) radiance from Imager onboard two geostationary Indian National Satellites (INSAT-3D and INSAT-3DR). This study also integrated different hydrometeors (like cloud, rain, ice, snow and graupel) as control variables in the WRF variation assimilation system. To do this, parallel experiments were performed by carrying out model simulations with and without INSAT WV radiance assimilation during July 2018. Results of these simulations suggested that the WRF model analyses for all-sky assimilation are closer to the brightness temperature ($\boldsymbol{T_B}$) of channel-1 (183.31 ± 0.2 GHz) of SAPHIR (Sondeur Atmosphérique du Profil d'Humidité Intertropicale par Radiométrie) sensor onboard Megha-Tropiques satellite and channel-3 (183.31 ± 1.0 GHz) of MHS (Microwave Humidity Sounder) sensor onboard National Oceanic and Atmospheric Administration (NOAA-18/19) and Meteorological Operational Satellite (MetOp-A/B/C) satellites. Furthermore, noteworthy changes are noticed in hydrometeors analyses with all-sky assimilation and the number of assimilated observations are increased significantly (around 2.5 times). The short-range predictions from all-sky assimilation runs revealed notable positive impact as compared to clear-sky assimilation runs when verified with SAPHIR and MHS $\boldsymbol{T}_B$, and NCEP (National Centers for Environmental Prediction) final analysis.

Keywords: *All sky, IR radiance, WRF model, Variational assimilation, Hydrometeors.*

1. Introduction

The advances in the numerical weather prediction (NWP) model represent a significant revolution in the scientific knowledge and technological advances in the last decades (Bauer et al. 2011a,b, 2015, 2021). The technical advancements has brought sea changes in the measurements of various parameters used in NWP model. Not only ground based measurements but also satellite measurements are increased significantly in both space and time. As a matter-of-fact, around 90-95% data assimilated in the NWP model are contributed by space-borne sensors. However, these satellite observations are still only 2 to 5% of measurements available globally and provided by satellites. The vast number of satellite data are not yet employed in the NWP model due to concurrent limitations of data assimilation methods like constraints of Gaussian assumption, uncorrelated observations, complex non-linearity, etc. (Kumar and Shukla, 2019). Condition of uncorrelated observations warrants data thinning whereas avoidance of surface channels due to unknown emissivity imposes the restriction of using channels that are sensitive to temperature (CO_2 and O_2 band) and water vapour (WV) (H_2O band) absorption, etc. in the assimilation system. Additionally, Around 75% of satellite measurements are discarded due to cloud contamination and unknown surface emissivity (Bauer et al. 2011a).

Presently, the Infrared (IR) measurements from satellites are assimilated with clear-sky limitations, and cloud removal or correction for IR radiance became a critical step for operational assimilation (Kumar and Shukla, 2019 and references therein). This cloud correction procedure also introduced representative error in the NWP model (Errico et al. 2007). The restriction of clear-sky assimilation is not due to insignificance of cloud-affected measurements, but mainly due to insufficient treatment of clouds in the radiative transfer (RT) models and inaccurate cloud parameters as first guess. Further, the intricacies of cloud affected IR radiances are exacerbated due to complex non-linearity in the cloud process. Furthermore, cloud parameters are not considered as part of control variables in most of the assimilation systems. The major cause of neglecting cloud parameters as control variables are due to large errors in the first-guess. In the last decade, the cloud and precipitation prediction from the NWP model has achieved a reasonable degree of realism that opens possibilities to explore impact of cloud-influenced radiance from IR and microwave (MW) sensors (Janisková, 2015), majorly high temporal and spatial resolution measurements from geostationary platform. Geer et al. (2019) discussed that the all-sky IR assimilation has not so far been operational at any weather forecasting centers that conveys requirements of new observations in critical cloud-affected regions and avoids cloud removing/clearing needs in future. Furthermore, the all-sky assimilation helped to avoid biases caused by undetected clouds that can affect the clear-sky assimilation (Geer et al. 2017, 2018).

Bauer et al. (2010) and Geer et al. (2010) demonstrated first successful direct assimilation of all-sky MW imager observations in the European Centre for Medium-Range Weather Forecasts (ECMWF) assimilation system. Authors also discussed the major concerns in the cloud and precipitation assimilation that include discontinuity in space and time, constraints of the present assimilation system that linearized the nonlinear processes, etc. Bauer et al. (2011b) reviewed development in the cloud affected satellite measurements in the operational NWP centers. Authors also discussed the need of the total moisture (e.g. WV, cloud liquid, cloud ice, and hydrometeors) as a control variable and generation of their background error covariance using National Meteorological Center (NMC; Parrish and Derber, 1992) method. Geer et al. (2017, 2018) highlighted that the cloud and precipitation data cannot be assimilated when missing in model first guess due to zero gradient problem and non-Gaussian distribution of error. Montmerle et al. (2010) also emphasized the necessity of background error modelling for clouds and precipitation parameters by ensemble forecast differences method. Zhang and Guan (2017) included cloud liquid, ice, and rain-water content as control variables in the assimilation of cloud-affected MW satellite measurements and found improvement in the model analysis. Chen et al. (2015) also suggested that the initialization of the cloud components in the NWP model is requisite because these quantities are resultant of atmospheric moisture and hydrometeor transport and complicated nonlinear physical processes associated with cloud development and decay. These previous studies highlighted that the inclusion of the different hydrometeors as control variables with their background error covariance is one of the major steps towards all-sky assimilation.

Recently, the efforts for assimilation in the NWP model has been more focused towards using clouds affected IR radiance, after remarkable success of the all-sky MW sensors and its operational implementation in many weather forecasting centers (e.g. Bauer et al., 2010; Geer et al., 2010; McNally, 2009; Pavelin et al., 2008; Eresmaa, 2014). Zhu et al. (2016) discussed operational assimilation of all-sky MW sensors in the National Oceanic and Atmospheric Administration (NOAA) National Centers for Environmental Prediction (NCEP) models. Various experiments have been performed in the last decade to explore the potential of assimilating all-sky IR radiance in the NWP model, majorly from geostationary satellites. Otkin (2010) assimilated window channel radiance for both clear-sky and cloudy-sky conditions at convection permitting scale and suggested that both observations are crucial for the NWP prediction. Okamoto et al. (2012) suggested to make use of a symmetric parameter, which is based upon observed and simulated cloud radiances. The use of symmetric parameter provided a better Gaussian form of background departure (observation minus background; O-B). Okamoto et al. (2014) and Harnisch et al. (2016) also proposed to use climatological error models for IR radiance as a function of different cloud-affected parameters. Zhang et al. (2018) assimilated all-sky IR observations from Geostationary Operational Environmental Satellite (GOES)-16 Advanced Baseline Imager (ABI) sensor using ensemble based data assimilation at convection allowing horizontal resolution. Zhang et al. (2016) also studied the potential impact of assimilating GOES-R radiance for tropical cyclone analysis using Ensemble Kalman Filter (EnKF) method. Minamide and Zhang (2018) explored the assimilation impact of all-sky IR radiance from the Himawari-8 satellite using the EnKF at convective scale for predicting super typhoon Soudelor. Authors suggested that the hourly update assimilation system improves initial intensity as well as spatial distribution of convective activities. Honda et al. (2018a) assimilated every 10-minutes all-sky radiance from Himawari-8 satellite for a case study of heavy rainfall. Honda et al. (2018b) also assimilated all-sky Himawari-8 IR radiance for soudelor typhoon, and found improved tropical cyclone structure and intensity prediction. Recently, Otkin and Potthast (2019) used an ensemble method to assimilate all-sky IR radiance from Spinning Enhanced Visible and InfraRed Imager (SEVIRI) sensor with different bias correction predictors and suggested improvement in short range forecasts.

The critical elements of all-sky IR/MW assimilations are inclusion of hydrometeor profiles in the RT model, use of cloud parameters as control variable, generation of cloud analysis increments using background error covariance for hydrometeors, radiance data information is mapped onto not only temperature and moisture fields, but also for different hydrometeors using Radiative Transfer Model (RTM) jacobians, etc. In the present study, first time all-sky IR WV radiance from the Indian geostationary satellites are assimilated in the weather research and forecasting (WRF) model with inclusion of hydrometeor profiles as control variables and their background errors using NMC method. Previously, Singh et al. (2016) assimilated clear-sky WV radiance from the INSAT-3D satellite in the WRF model and demonstrated positive impact on short-range weather prediction. In this study, three parallel experiments are performed during the entire month of July 2018 to understand the importance of all-sky assimilation. The WV channel data of Imager onboard INSAT-3D and INSAT-3DR satellites are described in section 2, and details about the WRF model and variational assimilation system are provided in section 3. Results and discussions are included in section 4, and concluded in the last section.

2. Data Description

2.1. INSAT-3D and INSAT-3DR Satellite

The Indian geostationary satellites INSAT-3D (Kumar and Shukla, 2019) and INSAT-3DR (Sankhala et al. 2020) are positioned at 82° E and 74° E at equator over the Indian Ocean, respectively. Both satellites carried two meteorological payloads including a very high-resolution radiometer (VHRR) also called Imager and an 18-channels IR sounder. The WV (6.5 - 7.1 um) channel is available in Imager, in addition to visible, short-wave IR, mid-IR, and two thermal IR channels. The INSAT-3D and

INSAT-3DR satellites collectively provide WV imagery at every 15 minutes in staggered mode at 8 km nominal spatial resolution. The calibration procedure of the multi-spectral Imager observations from INSAT-3D and INSAT-3DR satellites are broadly based on Weinreb et al. (1997). It is important to note that satellite instruments like INSAT-3D/3DR, which are in geostationary orbit and are three axis stabilized, face the problem of mid-night calibration. During mid-night, the Sun positioned directly opposite to the satellite and the Sun radiations intrude into the satellite aperture, and thus disturb the thermal equilibrium of the cavity of the satellite platform. IR instruments on-board are severely affected by such intrusion. This kind of problem was also observed in Kalpana-1 satellite (Shukla et al. 2012). The problem of direct sun radiation intrusion is more severe in INSAT-3D/3DR satellites because of its larger aperture size in comparison to Kalpana-1 satellite. Due to mid-night calibration issues a few acquisitions are discarded (or not taken) in case of INSAT-3D/3DR satellites. In the present study, WV channel radiance of INSAT-3D and INSAT-3DR satellites around 0300 UTC are used for assimilation study. This WV Imager radiance is available from satellite data archival centre at Space Applications Centre (SAC), Indian Space Research Organization (ISRO), Ahmedabad (http://www.mosdac.gov.in).

3. Methodology

The Advanced Research WRF (Skamarock et al. 2008) model version 4.2 and its three-dimensional variational (3D-Var) data assimilation system are used in this study to assess the impact of all-sky and clear-sky WV radiance assimilation. The diverse physics schemes are available in the WRF model for the treatment of convection and mesoscale precipitation systems, shortwave and longwave radiation, boundary layer processes, etc. The cumulus convection parameterization and planetary boundary layer of Kain–Fretcsh (KF) and Yonsei University (YSU) schemes, respectively are selected in this study. The rapid RT model for general circulation models (GCMs) (RRTMG) scheme is used for long-wave and short-wave radiation. The microphysics scheme used in this study is WRF Single-Moment 6-class (WSM6) scheme for microphysics. These schemes are selected based on their performances over the south Asia region (Kumar et al. 2014; Singh et al. 2016 and references therein). More details of design of experiments are available in Sankhala et al. (2020) and Kumar and Shukla (2019).

In the present study, three parallel assimilation experiments are performed with and without WV radiance assimilation from INSAT-3D and INSAT-3DR satellites during the entire month of July 2018. All set of experiments assimilated control observations that include conventional observations (like Synop, Sonde, Pilot, Ship, Aircraft, Buoy, etc.), atmospheric motion vectors from geostationary satellites, refractivity measurements from Global Positioning System (GPS) Radio Occultation (RO) available from NCEP Global Telecommunications System (GTS) at 0300 UTC. The 9-hour WRF model forecast, valid at 0300 UTC, is used as first guess for all sets of experiments. This procedure avoids the uncertainties whether these datasets are used in a global model assimilation system or not. The NCEP Global Data Assimilation System (GDAS) analysis at 0.25° × 0.25° spatial resolution is used to generate the lateral boundary conditions. The 48 hours WRF model forecasts are performed daily from 0300 UTC during 01-31 July 2018. The WRF model simulations are performed using a single domain having 12 km spatial resolution without cyclic assimilation. The model domain consists 700 × 700 grids covering regions of Latitude 25.7° S – 43.7° N and Longitude varies from 44.3° E to 119.7° E. The ***WCNT*** experiment defined as control run that assimilated control observations only, and no satellite radiances are assimilated in this experiment. The clear-sky and all-sky WV radiance from INSAT-3D and INSAT-3DR satellites are assimilated in the ***WCLR*** and ***WCLD*** experiments, respectively in addition to control observations.

The WRF 3D-Var data assimilation system is employed in this study for INSAT WV assimilation (Singh et al. 2016). A 1-h time window (±30-minutes) has been selected around the model initial time for assimilating control and satellite observations. Prior to data assimilation, all satellite data underwent a process of quality check to avoid the possibility of assimilating spurious observations. A strict quality control is performed, in which observations that differed from the model's first guess by more than three times the observational errors are removed. Here, observation error in the WV channel is assumed uncorrelated in space and time and the observational error covariance matrices are diagonal matrices with fix variance of 2.5 K for WV channel as diagonal element that may be a scope for future research to include separate observation errors for clear and cloudy radiance. The variational bias correction available in the WRF model is implemented to correct the biases in the radiance. In this study, the Community Radiative Transfer Model (CRTM; Han et al. 2006), a fast RT model, implemented in the WRF model, has been used for simulating the brightness temperature ($\boldsymbol{T_B}$) of WV channels of INSAT-3D and INSAT-3DR satellites. The CRTM model is a fast RT model developed by Joint Center for Satellite Data Assimilation (JCSDA). The CRTM model is widely used for data assimilation as a forward operator, and computation of gradient for various control variables (Zhang et al. 2018). To simulate the BT within WRF model, it uses the successive order of interaction (SOI) forward solver (Heidinger et al. 2006) using the OPTRAN (Optical Path Transmittance) code. For all-sky assimilation, a particle filter based cloud detection scheme for IR radiance with considering of cloud effects in CRTM calculations are implemented that are available in the WRF assimilation system (Xu et al. 2016). In this study, *cloud_cv_options=2* is considered which needs individual hydrometeor control variables with statistical error covariances. For this selection, in addition to standard control variables of stream function, unbalanced velocity potential, unbalanced temperature, unbalanced surface pressure and pseudo relative humidity, five different hydrometeors (cloud, rain, ice, snow, graupel) are also included as control variables for generalized background error covariance. The details of implementing generalized background error covariance are available in Descombes et al. (2015). Differences of 12- and 24-hour forecasts during the entire month of July 2018 are used to determine the background error covariance matrix by NMC method. In this study, cross-correlation for cloud and rain is considered with moisture, whereas no cross-correlation is considered for snow, ice and graupel mixing ratio.

4. Results and discussions

4.1. Impact in analysis

Figure 1 shows the spatial distribution of WV channel observations from the INSAT-3D satellite for a sample day at 0300 UTC 01 July 2018. The WV $\boldsymbol{T_B}$ from INSAT-3D satellite used in WCLR and WCLD runs are shown in figure 1(a) and figure 1(d), respectively. The CRTM model is used to prepare simulated $\boldsymbol{T_B}$ from the WRF model analysis, and further defined as simulated analyzed $\boldsymbol{T_B}$. Figure shows that a large number of observations are rejected in WCLR run (Fig. 1a), and this reduction is more prominent over land area. However, few WV observations are also rejected in the WCLD run (Fig. 1d) that are majorly due to strict quality control in variational method. For such cases, simulated WCLD analyzed $\boldsymbol{T_B}$ is far from INSAT-3D WV $\boldsymbol{T_B}$. These data gap regions in WCLD run suggested that the WRF simulated $\boldsymbol{T_B}$ with the CRTM model is still have differences with satellite measurements beyond the permissible limits due to various limitations of the NWP and RT model and satellite observations. It also indicates towards the need of separate observation error for clear and cloudy measurements. The first guess simulated WV $\boldsymbol{T_B}$ for WCLR (Fig. 1b) and WCLD (Fig. 1e) runs showed that the WRF model is able to capture the spatial distribution of observed $\boldsymbol{T_B}$. The simulated $\boldsymbol{T_B}$ matches relatively well over the ocean as compared to land due to imprecise land surface emissivity input in the RT modelling. The simulated analyzed $\boldsymbol{T_B}$ from the WCLR (Fig. 1c) and WCLD (Fig. 1f) runs clearly represented that the model analyses are closer to the INSAT-3D observed $\boldsymbol{T_B}$ as compared to first guess, which demonstrated the successful assimilation of the WV $\boldsymbol{T_B}$ in the WRF model. For all-sky (clear-sky) assimilation, the values of root-mean-square difference (defined as RMSD) is changed from 2.39 (1.42) K in background departure to 0.62 (0.59) K in analysis departure (observation minus analysis; O-A). Slightly larger values of mean difference (defined as BIAS) are found in WCLD analysis (-0.22 K) as compared to WCLR analysis (-0.19 K). It is important to note that the WCLD analysis is closer to cloud-affected satellite observation, which is generally not made use in clear-sky assimilation.

Figure 2 shows the spatial distribution of the mean first-guess and analysis departure for WCLR and WCLD runs during 1-31 July 2018 (total 31 sample days) for WV channel of INSAT-3D data. The spatial distribution of mean first guess departure in WCLR (Fig. 2a) and WCLD (Fig. 2b) runs showed almost similar distribution over the northern India and adjoining regions. However, large differences are seen over the

Indian Ocean that are mainly due to inclusion of cloud-affected radiance in WCLD runs. The mean analysis departure is reduced significantly for both WCLR (Fig. 2c) and WCLD (Fig. 2d) runs. It suggested that the INSAT-3D observed WV channel is successfully assimilated in the WRF model. The distribution of first guess and analysis departure for 1-31 July 2018 showed that the values of BIAS is reduced significantly from 0.19 K and -0.25 K in WCLR and WCLD first-guess departure to approximate zero in the analyses departure. The values of RMSD are reduced from 2.40 (1.33) K in WCLD (WCLR) first-guess to 0.60 (0.54) K in the analysis for INSAT-3D satellite. Similar statistics are found for INSAT-3DR satellite. These analyses clearly suggested that the WRF model analyses are closer to the satellite observed $\boldsymbol{T}_B$ for WV channel. Both, first-guess and analysis departure follows the Gaussian distribution for WCLD runs that suggested that incorporation of the hydrometeors as control variables do not influence the constraints of variational method (figure not shown). Few observations are rejected in the strict quality control, and varying observation errors for cloud-affected radiance may include these measurements and may be a scope for future research.

The temporal distribution of number of observations, domain average values of BIAS and RMSD for WCLR (in black colour) and WCLD (in grey colour) runs are shown in figure 3. The left (right) panel shows statistics for the INSAT-3D (INSAT-3DR) satellite. Figures 3(a) and 3(d) show the number of observations assimilated in the WCLR and WCLD runs from the INSAT-3D and INSAT-3DR satellites, respectively. Figure shows that more clear-sky observations are assimilated from the INSAT-3DR satellite (around 9820) as compared to INSAT-3D satellite (around 7630). However, no significant differences are found for the number of observations assimilated with all-sky for both satellites. The less value of BIAS is found in the analysis (dashed line) as compared to first-guess (solid line) for both WCLR and WCLD runs of INSAT-3D (Fig. 3b) and INSAT-3DR (Fig. 3e) satellites. For both satellites, WCLD (WCLR) first-guesses have a negative (positive) value of BIAS for most of the days. The RMSD values are reduced significantly for WCLD and WCNT analyses for both satellites. No significant differences are found between INSAT-3D (Fig. 3c) and INSAT-3DR (Fig. 3f) satellites. Furthermore, a slightly larger value of RMSD is found in WCLD analysis (0.73 K) as compared to WCNT analysis (0.52 K). These results clearly suggested that the all-sky observations are successfully assimilated in the WRF model with additional control variables of hydrometeors.

Figure 4 shows the spatial distribution of the anomaly in WCLD and WCNT analyses (defined WCLD minus WCNT) for different parameters at 500 hPa during July 2018. The spatial distribution of anomaly for WV mixing ratio (Fig. 4a) shows significant differences over the model domain. These differences are majorly over the mid- and high vertical levels (around 600 to 200 hPa) which are majorly due to sensitivity of INSAT-3D/3DR WV channel over these atmospheric layers (Kumar et al. 2012). Due to multivariate nature of variation assimilation, mean departure for temperature (Fig. 4b), zonal winds (Fig. 4c) and meridional winds (Fig. 4d) are also changed spatially over the model domain. These differences are larger over the land for zonal and meridional winds. These differences are also available at different vertical levels that are more dominant in the upper atmosphere (above 400 hPa) (figure not shown due to brevity). Furthermore, the control variables of different hydrometeors also show significant differences in different atmospheric layers. The spatial distribution of cloud mixing ratio (Fig. 4e) and rain-mixing ratio (Fig. 4f) show major differences over the landmass and the Bay of Bengal regions. These differences are high in the lower layers of the atmosphere (figure not shown due to brevity). The spatial distribution of snow (Fig. 4g), ice (Fig. 4h), and graupel (Fig. 4i) mixing ratio shows noteworthy changes at 500 hPa over model domain. In general, due to absence of these hydrometeors as control variables, these changes are not possible in the model analysis. The changes in snow, ice and graupel mixing ratio are prominent over mid- and upper-atmospheric layers.

To evaluate the impact of INSAT-3D/3DR WV radiance assimilation in the WCLR and WCLD runs as compared to WCNT runs, the WRF model analyses are also compared with satellite observations that are not used for data assimilation. The channel-1 (183.31 $\pm$ 0.2 GHz) $\boldsymbol{T_B}$ from SAPHIR (Sondeur Atmosphérique du Profil d'Humidité Intertropicale par Radiométrie) sensor onboard Megha-Tropiques satellite (Fig. 5) and channel-3 (183.31 $\pm$ 1.0 GHz) of MHS (Microwave Humidity Sounder) onboard NOAA-18/19 and Meteorological Operational Satellite (MetOp)-A/B/C (Fig. 6) are used here. The selected WV channel of SAPHIR and MHS sensors are also sensitive to upper atmospheric layers (500 to 150 hPa) and can be utilized to evaluate the WCLR and WCLD analyses. The mean SAPHIR $\boldsymbol{T_B}$ observations are shown in figure 5(a). Due to the low-inclination (~20°) orbit of Megha-Tropiques satellite, the WRF model analyses are compared upto ~30° N of the study domain. It shows less value of $\boldsymbol{T_B}$ over the Indian landmass and adjoining oceanic regions that generally occurred during the summer monsoon period. The RMSD in the WCNT analysis simulated $\boldsymbol{T_B}$ against SAPHIR observations are shown in figure 5(b). Large differences are found over the active monsoon regions, mainly the Bay of Bengal, Indo Gangetic Plain, and ITCZ (Inter Tropical Convergence Zone) regions. Slightly larger RMSD values are found over land, coastal and adjoining oceanic regions. An improvement parameter is defined here to understand the impact of WCLR or WCLD experiments over WCNT experiments. The improvement parameter for clear-sky and all-sky are defined as

$$\alpha_{CLR} = \sqrt{\sum_{i=1}^{N}(BT_{WCNT} - BT_{SAT})^2} - \sqrt{\sum_{i=1}^{N}(BT_{WCLR} - BT_{SAT})^2} \qquad (1)$$

$$\alpha_{CLD} = \sqrt{\sum_{i=1}^{N}(BT_{WCNT} - BT_{SAT})^2} - \sqrt{\sum_{i=1}^{N}(BT_{WCLD} - BT_{SAT})^2} \qquad (2)$$

The improvement parameter for clear-sky and all-sky analyses are defined as α_{CLR} and α_{CLD}, respectively. The parameters BT_{SAT}, BT_{WCNT}, BT_{WCLR}, and BT_{WCLD} are $\boldsymbol{T_B}$ from satellite, and simulated $\boldsymbol{T_B}$ from WCNT, WCLR, and WCLD runs, respectively. The *N* is the total number of sample days that are 31 in this study. The positive (negative) values of improvement parameter shows improvement (degradation) of WV assimilation over WCNT experiments. The spatial distribution of improvement parameter for WCLR and WCLD runs are shown in figure 5(c) and figure 5(d), respectively. In general, both clear-sky and all-sky assimilation has a positive impact on the WRF model analyses. However, small degradation is also seen over the western part of India and Arabian Sea in WCLR runs, and southern India and Bay of Bengal regions in WCLD runs. The positive improvements are more prominent over the ITCZ regions in WCLD runs. Results suggest larger improvement in WCLD runs as compared to WCLR runs that show the importance of all-sky assimilation in the model analyses. It is also interesting to note that larger improvements are seen over the land in the WCLD runs as compared to WCLR runs. Furthermore, results are extended for high-latitude regions that are not possible with SAPHIR observation. For this purpose, similar analyses are also prepared with channel-3 measurements of MHS sensors that are also sensitive to upper layers of atmospheric moisture. The mean value of MHS measured $\boldsymbol{T_B}$ is shown in figure 6(a) that re-confirm the low values of $\boldsymbol{T_B}$ over core monsoon regions as shown in figure 5(a) for SAPHIR data. The WCNT simulated $\boldsymbol{T_B}$ has a large value of RMSD over the landmass, ITCZ, and Bay of Bengal regions (Fig. 6b). A noteworthy high RMSD is seen over the northern part of the domain majorly over Jammu and Kashmir and nearby regions. The spatial distribution of improvement parameter shows positive impact of clear-sky assimilation over the oceanic regions. Moreover, large RMSD errors over the ITCZ regions are also improved with assimilation of clear-sky $\boldsymbol{T_B}$ (Fig. 6c). However, the value of improvement parameter is slightly negative over Indian landmass. The improvement parameter for all-sky assimilation are noteworthy positive over the ITCZ regions. Furthermore, WCLD analyses have shown larger impact over the landmass as compared to WCLR analyses. These large improvements in WCLD analyses are majorly due to cloud-affected radiance that are not used for WCLR runs. Overall, these results based on one-month experiments suggested that all-sky assimilation is successfully implemented in the WRF model with additional control variables of different hydrometeors. Moreover, the verifications of the WRF model analyses with independent MW satellite observations suggested that the WCLD analyses are more realistic and accurate as compared to WCLR and WCNT analyses. These positive impacts in model analyses are further evaluated for short-range weather prediction in the section 4.2.

4.2. Impact in forecast

To assess the impact of clear-sky and all-sky assimilation, three-hourly forecasts from the WRF model (upto 48 hours) are compared with SAPHIR and MHS observed $\boldsymbol{T_B}$, and NCEP final moisture analyses. The distribution of number of observations used for improvement parameter computation are shown in figure 7(a) and figure 8(a) for SAPHIR and MHS sensors, respectively. The number of observations are almost twice in MHS due to availability on various platforms and global coverage. Figure 7(b) clearly shows that the value of RMSD in WCNT runs increases with forecast lengths. Minimum RMSD error is found in first 12 hours forecasts and reaches maximum after 24 hours. However, the RMSD in WCNT shows diurnal variations in errors when compared with MHS observations (Fig. 8b). The maximum errors are observed at 0900 UTC (in 06-hour forecasts) and 2100 UTC (in 18-hour forecasts), when the number of MHS observations are least. Similar to SAPHIR comparison, the RMSD values are increased with forecast lengths in figure 8(b). The percentage improvement parameter for WCLR and WCLD forecasts against WCNT forecasts are shown in figure 7(c) and figure 7(d), respectively for SAPHIR observations, and in figure 8(c) and figure 8(d), respectively for MHS observations. Results show that clear-sky assimilation has positive impact on short range prediction, this positive improvement is more prominent when all-sky observations are assimilated in the WRF model. This improvement is higher than 5-10% for short-range forecasts when compared with SAPHIR observations. Figures 8(c,d) show that the value of positive improvement is reduced rapidly after a few hours and neutral to marginal positive impact is seen for both WCLR and WCLD runs. The possible cause of this reduction in positive improvement may be due to strict quality control in data assimilation. Kumar et al. (2014) also mentioned that the strict quality control in data assimilation improves short-range forecast only. Another possible reason may be due to identical lateral boundary conditions without cyclic assimilation that may also influence the longer forecasts.

The spatial distribution of the mean WV mixing ratio at upper vertical level (300 hPa) from the NCEP final analysis and 12-hour forecasts from the WCNT runs are shown in figure 9(a) and figure 9(b), respectively. Figure shows that the WCNT runs are able to capture spatial distribution of upper level moisture with few differences over the central India and orographic regions. The spatial distribution of percentage improvement parameter for WCLR runs show almost neutral impact of clear-sky assimilation, except in the northern part of the study domain (Fig. 9c). The spatial distribution of percentage improvement parameter in WCLD runs against WCNT runs suggested noteworthy improvements over the central India, northern and western Arabian Sea regions. Few pockets of positive improvement can also be seen over the Indian Ocean. Vertical profile of improvement suggests that the maximum positive impact occurs over the upper layer of atmosphere (Fig. 10). These positive improvements reduce with forecast lengths for WCLD runs (Fig. 10b). These positive improvements are less in magnitude for WCLR runs (Fig. 10a) and majorly exist over the mid-layer of atmosphere (600 to 250 hPa) for all forecast lengths upto 48 hours. The magnitude of negative impact is also seen at surface and upper layers (around 100 hPa) in all-sky assimilation. This negative impact is almost negligible for clear-sky assimilation. Overall, these results suggested that the WRF model predictions improve with all-sky assimilation as compared to clear-sky assimilation.

5. Conclusion

In this study, the assimilation of clear-sky and all-sky IR observations from WV channel of Imager onboard INSAT-3D and INSAT-3DR satellites are assimilated in the WRF model using variational method. The different hydrometeors are considered as individual control variables to understand the importance of clouds as control variables. The background error covariance matrix for different control variables using the NMC method is implemented in the 3D-Var assimilation system. The changes in different hydrometeors analyses suggested that this assimilation system is able to modify the initial state of hydrometeors in the WRF model. It is clearly demonstrated that the all-sky analyses are closer to the independent satellite observations as compared to analyses from WCLR and WCNT runs. This study demonstrats that the all-sky IR WV observations are able to improve the moisture information over the study domain that are very crucial over the south-Asia regions. Overall, results suggested that the analysis as well as forecasts from the WCLD runs are closer to observations and final analysis as compared to WCLR and WCNT runs. Results show the potential of assimilating all-sky measurements from IR sensors on-board geostationary satellites. This study did not consider the importance of frequent sampling from geostationary satellites that may be a scope for further research using WRF four-dimensional variational (4D-Var) or four-dimensional ensemble variational (4DEnVar) in future. Additional research is needed to understand the degradation of positive impact with forecast lengths in all-sky assimilation.

Acknowledgement

Authors are thankful to Dr. P. K. Thapliyal, Head, GRD/AOSG/EPSA, Space Applications Centre, ISRO for various discussions related to INSAT-3D/3DR satellites. Authors are also thankful to Dr. Randhir Singh for providing WRF code published in Singh et al. (2016) for clear-sky assimilation of INSAT-3D satellite. The INSAT-3D and INSAT-3DR data are available from www.mosdac.gov.in. Authors acknowledge the WRF model and its assimilation system available from www2.mmm.ucar.edu/wrf/src/ repository. Thanks are also due to CISL-RDA for providing the NCEP global model analysis, PREPbufr data, and GPS RO data used in this study from https://rda.ucar.edu/ data sets. The model simulations are too large to include as supporting information.

References

Bauer, P., Geer, A.J., Lopez, P. and Salmond, D., 2010. Direct 4D-Var assimilation of all-sky radiances. Part I: Implementation. *Quarterly Journal of the Royal Meteorological Society*, *136*(652), pp.1868-1885.

Bauer, P., Ohring, G., Kummerow, C. and Auligne, T., 2011. Assimilating satellite observations of clouds and precipitation into NWP models. *Bulletin of the American Meteorological Society*, *92*(6), pp.ES25-ES28.

Bauer, P., Auligné, T., Bell, W., Geer, A., Guidard, V., Heilliette, S., Kazumori, M., Kim, M.J., Liu, E.H.C., McNally, A.P. and Macpherson, B., 2011. Satellite cloud and precipitation assimilation at operational NWP centres. *Quarterly Journal of the Royal Meteorological Society*, *137*(661), pp.1934-1951.

Bauer, P., Thorpe, A. and Brunet, G., 2015. The quiet revolution of numerical weather prediction. *Nature*, *525*(7567), pp.47-55.

Bauer, P., Dueben, P.D., Hoefler, T., Quintino, T., Schulthess, T.C. and Wedi, N.P., 2021. The digital revolution of Earth-system science. *Nature Computational Science*, *1*(2), pp.104-113.

Chen, Y., Wang, H., Min, J., Huang, X.Y., Minnis, P., Zhang, R., Haggerty, J. and Palikonda, R., 2015. Variational assimilation of cloud liquid/ice water path and its impact on NWP. *Journal of Applied Meteorology and Climatology*, *54*(8), pp.1809-1825.

Descombes, G., Auligné, T., Vandenberghe, F., Barker, D.M. and Barré, J., 2015. Generalized background error covariance matrix model (GEN_BE v2. 0). *Geoscientific Model Development*, *8*(3), pp.669-696.

Eresmaa, R., 2014. Imager-assisted cloud detection for assimilation of Infrared Atmospheric Sounding Interferometer radiances. *Quarterly Journal of the Royal Meteorological Society*, *140*(684), pp.2342-2352.

Errico, R.M., Bauer, P. and Mahfouf, J.F., 2007. Issues regarding the assimilation of cloud and precipitation data. *Journal of the Atmospheric Sciences*, *64*(11), pp.3785-3798.

Geer, A.J., Bauer, P. and Lopez, P., 2010. Direct 4D-Var assimilation of all-sky radiances. Part II: Assessment. *Quarterly Journal of the Royal Meteorological Society*, *136*(652), pp.1886-1905.

Geer, A.J., Baordo, F., Bormann, N., Chambon, P., English, S.J., Kazumori, M., Lawrence, H., Lean, P., Lonitz, K. and Lupu, C., 2017. The growing impact of satellite observations sensitive to humidity, cloud and precipitation. *Quarterly Journal of the Royal Meteorological Society*, *143*(709), pp.3189-3206.

Geer, A.J., Lonitz, K., Weston, P., Kazumori, M., Okamoto, K., Zhu, Y., Liu, E.H., Collard, A., Bell, W., Migliorini, S. and Chambon, P., 2018. All-sky satellite data assimilation at operational weather forecasting centres. *Quarterly Journal of the Royal Meteorological Society*, *144*(713), pp.1191-1217.

Geer, A.J., Migliorini, S. and Matricardi, M., 2019. All-sky assimilation of infrared radiances sensitive to mid-and upper-tropospheric moisture and cloud. *Atmospheric Measurement Techniques*, *12*(9), pp.4903-4929.

Han, Y., van Delst, P., Liu, Q., Weng, F., Yan, B., Treadon, R. and Derber, J., 2006. JCSDA Community Radiative Transfer Model–Version 1 (CRTM-V1). *NESDIS: NOAA Tech. Rep*, p.40.

Harnisch, F., Weissmann, M. and Periáñez, Á., 2016. Error model for the assimilation of cloud-affected infrared satellite observations in an ensemble data assimilation system. *Quarterly Journal of the Royal Meteorological Society*, *142*(697), pp.1797-1808.

Heidinger, A.K., O'Dell, C., Bennartz, R. and Greenwald, T., 2006. The successive-order-of-interaction radiative transfer model. Part I: Model development. *Journal of applied meteorology and climatology*, *45*(10), pp.1388-1402.

Honda, T., Kotsuki, S., Lien, G.Y., Maejima, Y., Okamoto, K. and Miyoshi, T., 2018a. Assimilation of Himawari-8 all-sky radiances every 10 minutes: Impact on precipitation and flood risk prediction. *Journal of Geophysical Research: Atmospheres*, *123*(2), pp.965-976.

Honda, T., Miyoshi, T., Lien, G.Y., Nishizawa, S., Yoshida, R., Adachi, S.A., Terasaki, K., Okamoto, K., Tomita, H. and Bessho, K., 2018b. Assimilating all-sky Himawari-8 satellite infrared radiances: A case of Typhoon Soudelor (2015). *Monthly Weather Review*, *146*(1), pp.213-229.

Janisková, M., 2015. Assimilation of cloud information from space-borne radar and lidar: experimental study using a 1D+ 4D-Var technique. *Quarterly Journal of the Royal Meteorological Society*, *141*(692), pp.2708-2725.

Kumar, P., Shukla, M.V., Thapliyal, P.K., Bisht, J.H. and Pal, P.K., 2012. Evaluation of upper tropospheric humidity from NCEP analysis and WRF Model Forecast with Kalpana observation during Indian summer monsoon 2010. *Meteorological Applications*, 19(2), pp.152-160.

Kumar, P., Kishtawal, C.M. and Pal, P.K., 2014. Impact of satellite rainfall assimilation on Weather Research and Forecasting model predictions over the Indian region. *Journal of Geophysical Research: Atmospheres*, *119*(5), pp.2017-2031.

Kumar, P. and Shukla, M.V., 2019. Assimilating INSAT-3D thermal infrared window imager observation with the particle filter: A case study for Vardah Cyclone. *Journal of Geophysical Research: Atmospheres*, *124*(4), pp.1897-1911.

McNally, A.P., 2009. The direct assimilation of cloud-affected satellite infrared radiances in the ECMWF 4D-Var. *Quarterly Journal of the Royal Meteorological*

Society: A journal of the atmospheric sciences, applied meteorology and physical oceanography, *135*(642), pp.1214-1229.

Minamide, M. and Zhang, F., 2018. Assimilation of all-sky infrared radiances from Himawari-8 and impacts of moisture and hydrometer initialization on convection-permitting tropical cyclone prediction. *Monthly Weather Review*, *146*(10), pp.3241-3258.

Montmerle, T., Michel, Y. and Ménétrier, B., 2010. Modelling of background error covariances for the analysis of clouds and precipitation. In *Proceedings of the ECMWF-JCSDA Workshop on Assimilating Satellite Observations of Clouds and Precipitation* (p. 10).

Okamoto, K., McNally, A.P. and Bell, W., 2012. *Cloud information from high spectral resolution IR sounders*. NWPSAF-EC-VS-022. http://research. metoffice. gov. uk/research/interproj/nwpsaf/vs. html (accessed 25 October 2013).

Okamoto, K., McNally, A.P. and Bell, W., 2014. Progress towards the assimilation of all-sky infrared radiances: an evaluation of cloud effects. *Quarterly Journal of the Royal Meteorological Society*, *140*(682), pp.1603-1614.

Otkin, J.A., 2010. Clear and cloudy sky infrared brightness temperature assimilation using an ensemble Kalman filter. *Journal of Geophysical Research: Atmospheres*, *115*(D19).

Otkin, J.A. and Potthast, R., 2019. Assimilation of all-sky SEVIRI infrared brightness temperatures in a regional-scale ensemble data assimilation system. *Monthly Weather Review*, *147*(12), pp.4481-4509.

Parrish, D.F. and Derber, J.C., 1992. The National Meteorological Center's spectral statistical-interpolation analysis system. *Monthly Weather Review*, *120*(8), pp.1747-1763.

Pavelin, E.G., English, S.J. and Eyre, J.R., 2008. The assimilation of cloud-affected infrared satellite radiances for numerical weather prediction. *Quarterly Journal of the Royal Meteorological Society: A journal of the atmospheric sciences, applied meteorology and physical oceanography*, *134*(632), pp.737-749.

Sankhala, D.K., Deb, S.K., Kumar, P. and Kishtawal, C.M., 2020. Retrieval and application of high-resolution low-level visible winds from INSAT-3DR imager. *International Journal of Remote Sensing*, *41*(12), pp.4726-4741.

Singh, R., Ojha, S.P., Kishtawal, C.M., Pal, P.K. and Kiran Kumar, A.S., 2016. Impact of the assimilation of INSAT-3D radiances on short-range weather forecasts. *Quarterly Journal of the Royal Meteorological Society*, *142*(694), pp.120-131.

Shukla, M.V., Thapliyal, P.K., Bisht, J.H., Mankad, K.N., Pal, P.K. and Navalgund, R.R., 2012. Intersatellite calibration of Kalpana thermal infrared channel using AIRS hyperspectral observations. *IEEE Geoscience and Remote Sensing Letters*, *9*(4), pp.687-689.

Skamarock, W.C., Klemp, J.B., Dudhia, J., Gill, D.O., Barker, D.M., Wang, W. and Powers, J.G., 2008. A description of the Advanced Research WRF version 3. NCAR Technical note-475+ STR.

Weinreb, M., Jamieson, M., Fulton, N., Chen, Y., Johnson, J.X., Bremer, J., Smith, C. and Baucom, J., 1997. Operational calibration of Geostationary Operational Environmental Satellite-8 and-9 imagers and sounders. *Applied optics*, *36*(27), pp.6895-6904.

Xu, D., Auligné, T., Descombes, G. and Snyder, C., 2016. A method for retrieving clouds with satellite infrared radiances using the particle filter. *Geoscientific Model Development*, *9*(11), pp.3919-3932.

Zhang, F., Minamide, M. and Clothiaux, E.E., 2016. Potential impacts of assimilating all-sky infrared satellite radiances from GOES-R on convection-permitting analysis and prediction of tropical cyclones. *Geophysical Research Letters*, *43*(6), pp.2954-2963.

Zhang, S. and Guan, L., 2017. Preliminary study on direct assimilation of cloud-affected satellite microwave brightness temperatures. *Advances in Atmospheric Sciences*, *34*(2), pp.199-208.

Zhang, Y., Zhang, F. and Stensrud, D.J., 2018. Assimilating all-sky infrared radiances from GOES-16 ABI using an ensemble Kalman filter for convection-allowing severe thunderstorms prediction. *Monthly Weather Review*, *146*(10), pp.3363-3381.

Zhu, Y., Liu, E., Mahajan, R., Thomas, C., Groff, D., Van Delst, P., Collard, A., Kleist, D., Treadon, R. and Derber, J.C., 2016. All-sky microwave radiance assimilation in NCEP's GSI analysis system. *Monthly Weather Review*, *144*(12), pp.4709-4735.

Figure captions

Figure 1: Spatial distribution of INSAT-3D WV $\boldsymbol{T_B}$ observations assimilated in the (a) WCLR and (d) WCLD runs, simulated $\boldsymbol{T_B}$ from (b) WCLR first guess, (c) WCLR analysis, (e) WCLD first guess, and (f) WCLD analysis on a sample day 01 July 2018.

Figure 2: Spatial distribution of average first-guess departure for (a) WCLR and (b) WCLD runs, and analysis departure for (c) WCLR and (d) WCLD runs during 1-31 July 2018.

Figure 3: Temporal distribution of number of observations assimilated in WCLR and WCLD runs for (a) INSAT-3D and (d) INSAT-3DR satellites, BIAS in first-guess and analysis for (b) INSAT-3D and (e) INSAT-3DR satellites, and RMSD in first-guess and analysis for (c) INSAT-3D and (f) INSAT-3DR satellites during July 2018. The WCLR and WCLD runs are defined as CLR and CLD, respectively. First-guess and analysis are shown as solid-line and dash-line, respectively.

Figure 4: Spatial distribution of anomaly (WCLD – WCNT) analyses for variables (a) humdity (g Kg^{-1}), (b) temperature (°C), (c) Zonal wind (m s^{-1}), (d) meridional wind (m s^{-1}), (e) cloud mixing ratio (mg Kg^{-1}), (f) rain mixing ratio (mg Kg^{-1}), (g) snow mixing ratio (mg Kg^{-1}), (h) ice mixing ratio (mg Kg^{-1}), and (i) graupel mixing ratio (mg Kg^{-1}) variables at 500 hPa during July 2018.

Figure 5: Spatial distribution of (a) mean SAPHIR channel-1 $\boldsymbol{T_B}$, (b) RMSD in the WCNT simulated $\boldsymbol{T_B}$ against SAPHIR, improvement parameter (K) in (c) WCLR and

(d) WCLD simulated analyzed $\boldsymbol{T}_B$ against WCNT simulated analyzed $\boldsymbol{T}_B$ during entire month of July 2018.

Figure 6: Spatial distribution of (a) mean MHS channel-3 $\boldsymbol{T}_B$, (b) RMSD in the WCNT simulated $\boldsymbol{T}_B$ against MHS, improvement parameter (K) in (c) WCLR and (d) WCLD simulated analyzed $\boldsymbol{T}_B$ against WCNT simulated analyzed $\boldsymbol{T}_B$ during entire month of July 2018.

Figure 7: Spatial distribution of (a) number of SAPHIR observations used for 03-hourly forecasts verifications, (b) RMSD in WCNT forecasts simulated $\boldsymbol{T}_B$ against SAPHIR, percentage improvement parameter in (c) WCLR and (d) WCLD forecasts simulated $\boldsymbol{T}_B$ against WCNT forecasts simulated $\boldsymbol{T}_B$ during 1-31 July 2018.

Figure 8: Spatial distribution of (a) number of MHS observations used for 03-hourly forecasts verifications, (b) RMSD in WCNT forecasts simulated $\boldsymbol{T}_B$ against MHS, percentage improvement parameter in (c) WCLR and (d) WCLD forecasts simulated $\boldsymbol{T}_B$ against WCNT forecasts simulated $\boldsymbol{T}_B$ during 1-31 July 2018.

Figure 9: Spatial distribution of WV mixing ratio from (a) NCEP final analysis, and (b) 12-hour forecast from WCNT runs, percentage improvement parameter for (c) WCLR and (d) WCLD runs against WCNT runs at 300 hPa during July 2018.

Figure 10: Time-Height plot of percentage improvement parameter for different forecast lengths for (a) WCLR and (d) WCLD runs against WCNT runs, when compared with NCEP final analysis during the entire month of July 2018.

Figure 01.

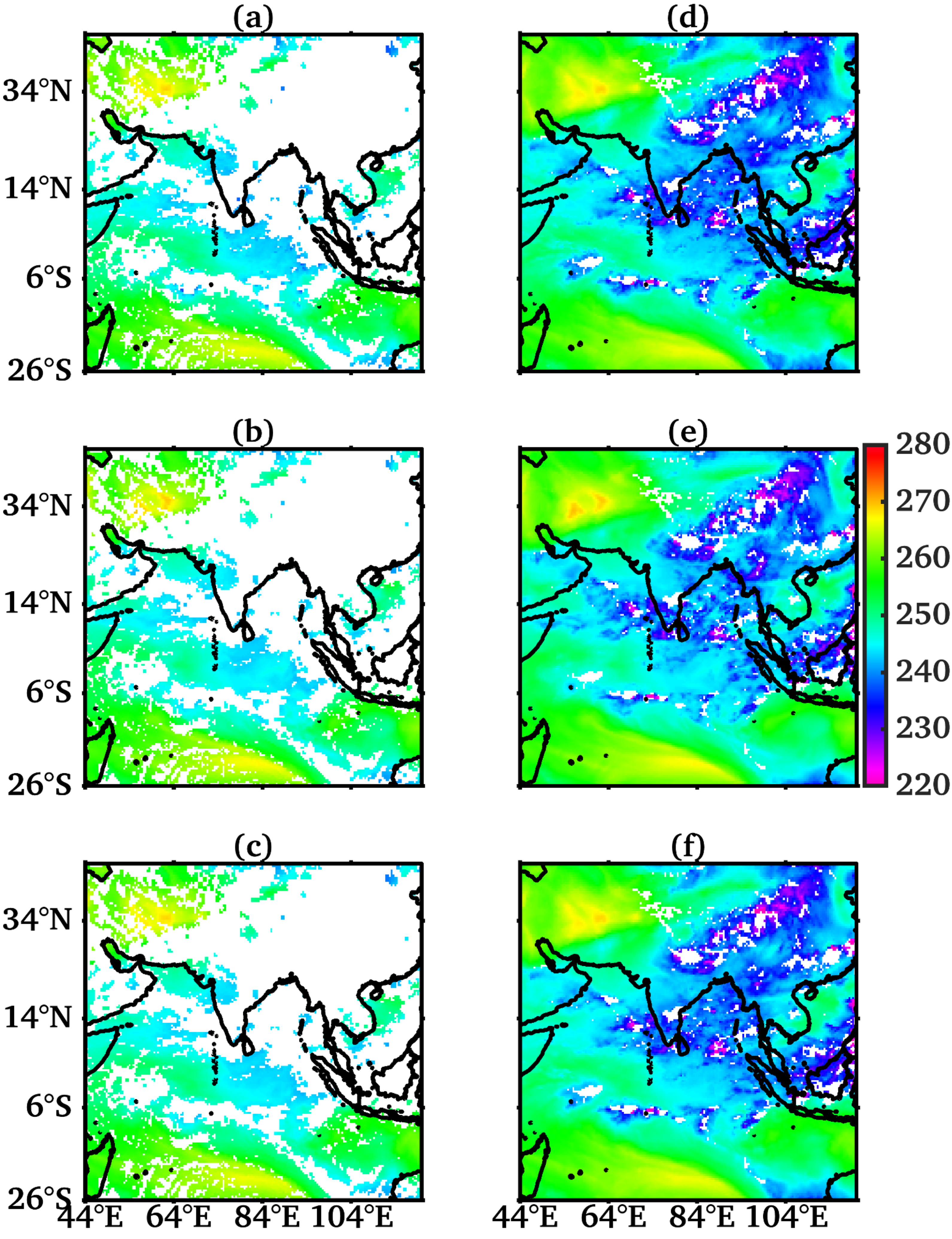

(a)
(d)
(b)
(e)
(c)
(f)
34°N
14°N
6°S
26°S
44°E
64°E
84°E
104°E
280
270
260
250
240
230
220

Figure 02.

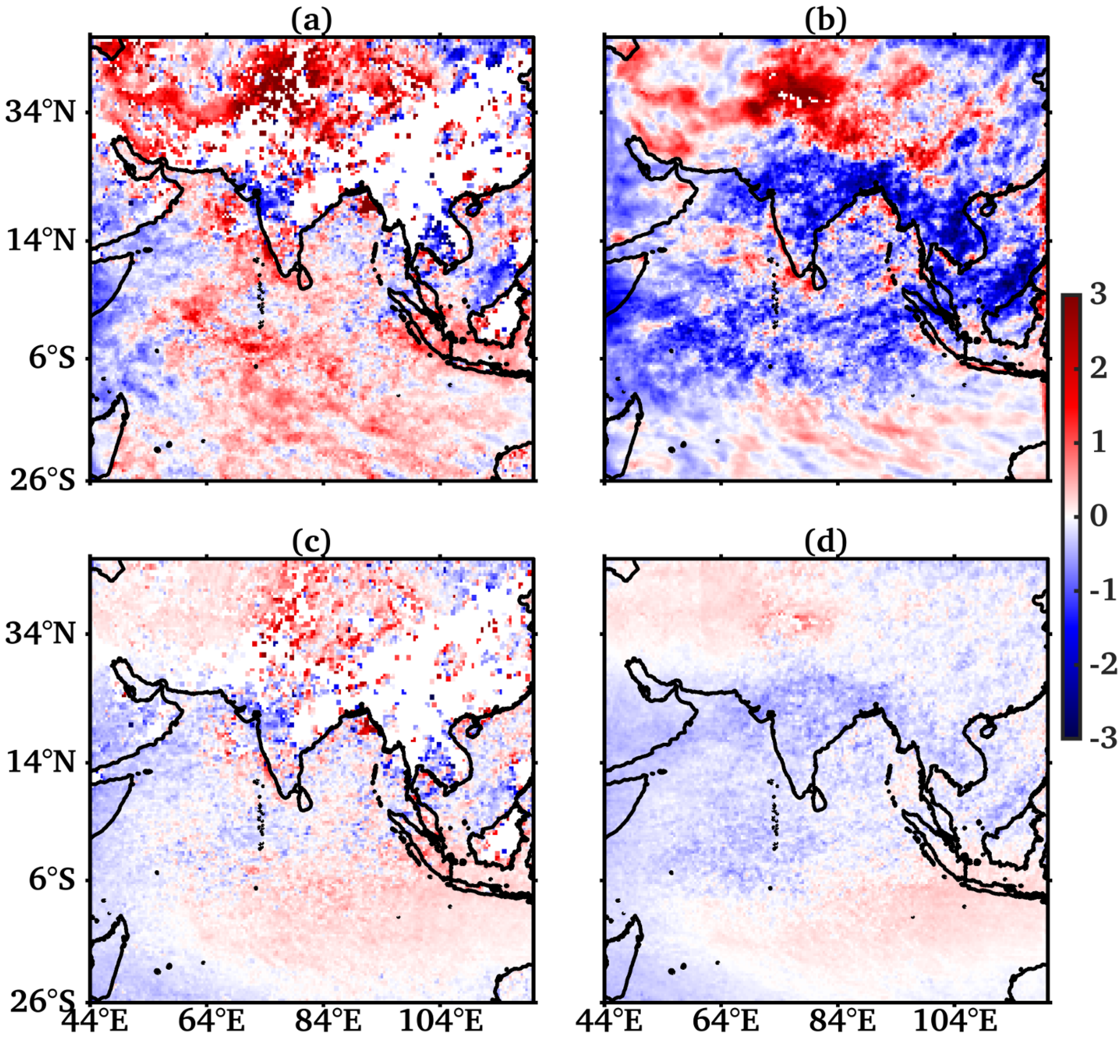
(a)
(b)
(c)
(d)
34°N
14°N
6°S
26°S
44°E
64°E
84°E
104°E
3
2
1
0
-1
-2
-3

Figure 03.

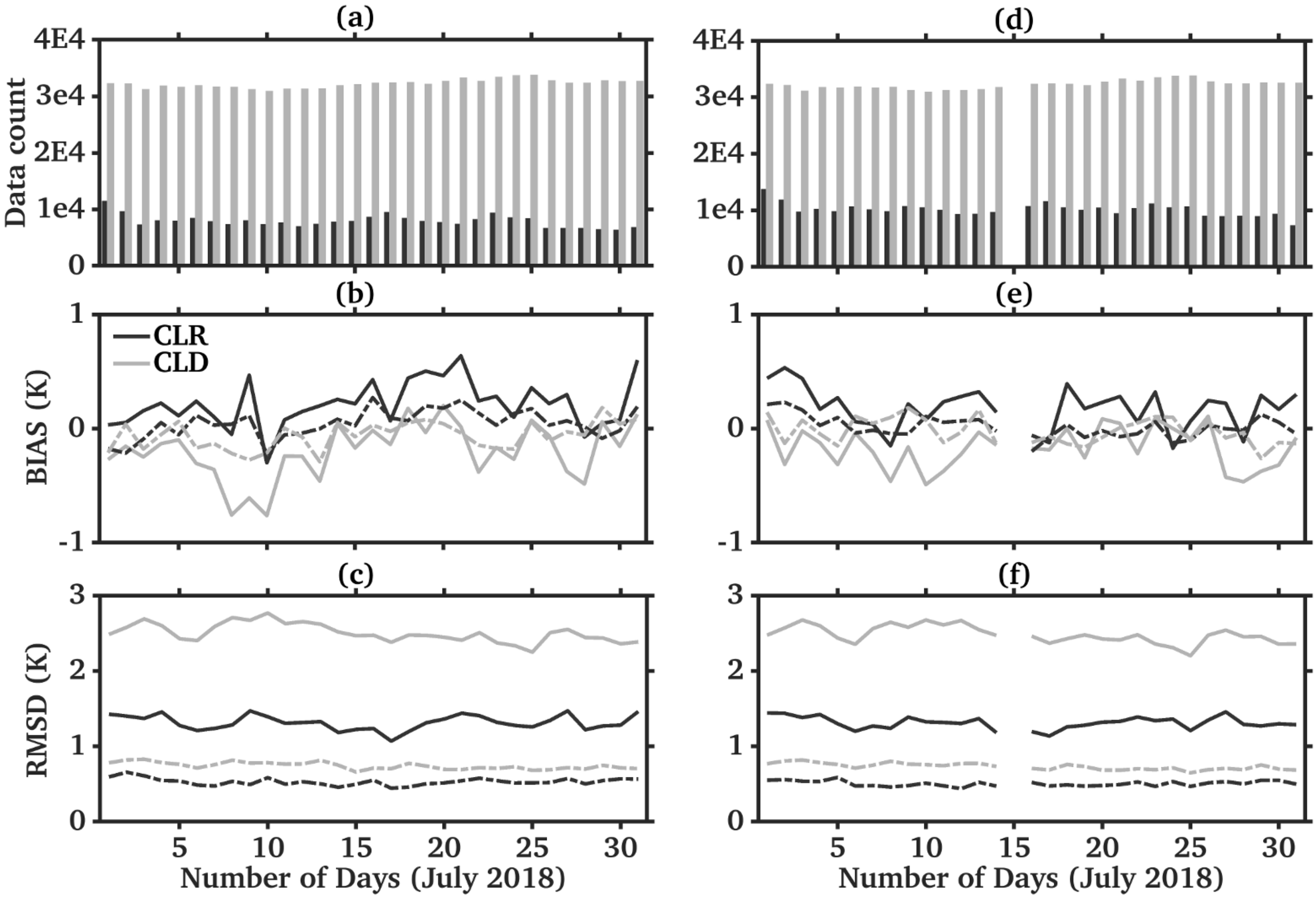

(a)
(b)
(c)
(d)
(e)
(f)
Data count
4E4
3e4
2E4
1e4
0
BIAS (K)
1
0
-1
CLR
CLD
RMSD (K)
3
2
1
0
5
10
15
20
25
30
Number of Days (July 2018)
Number of Days (July 2018)

Figure 04.

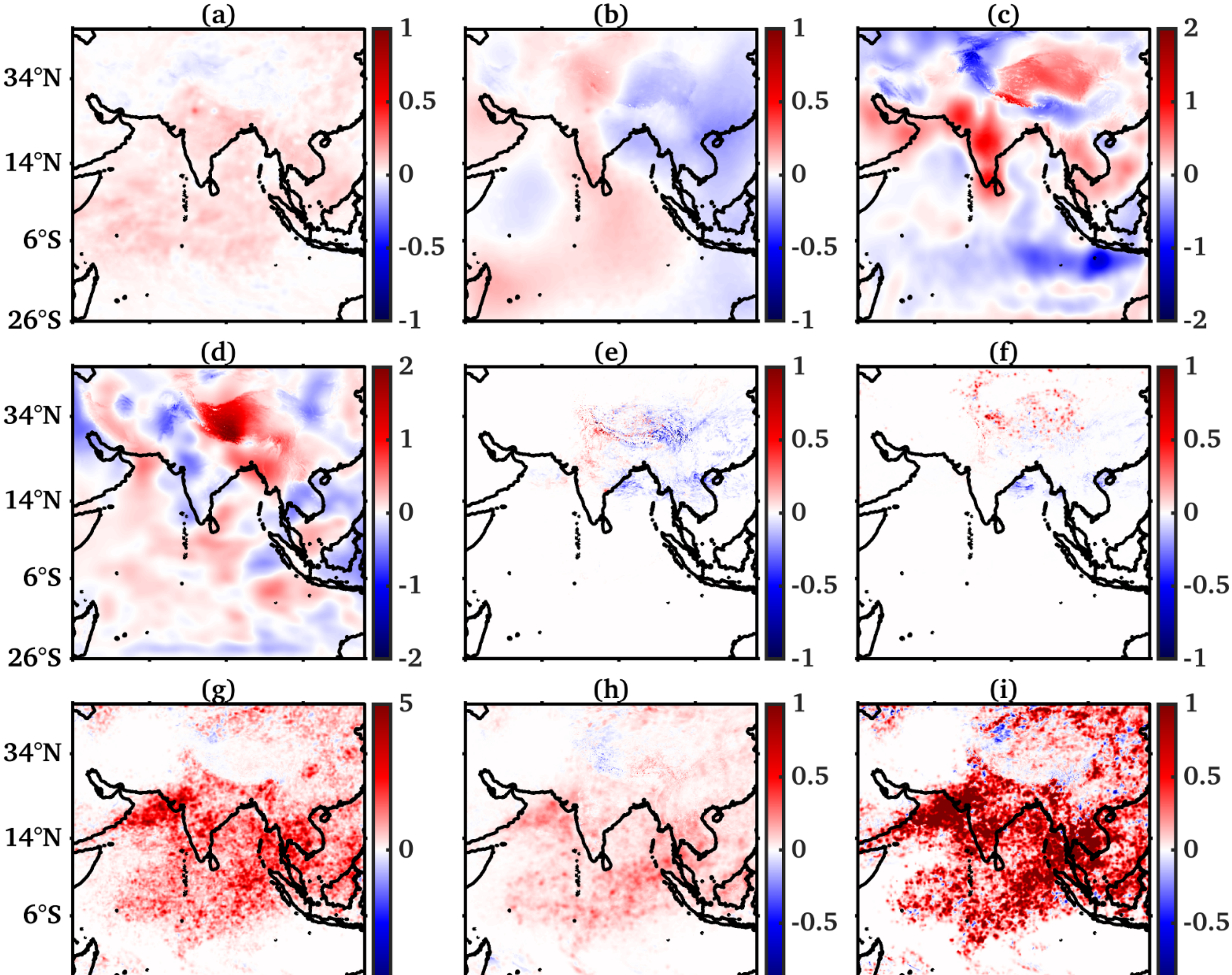

(a)
(b)
(c)
(d)
(e)
(f)
(g)
(h)
(i)
34°N
14°N
6°S
26°S
44°E
64°E
84°E
104°E
1
0.5
0
-0.5
-1
2
-2
5
-5

Figure 05.

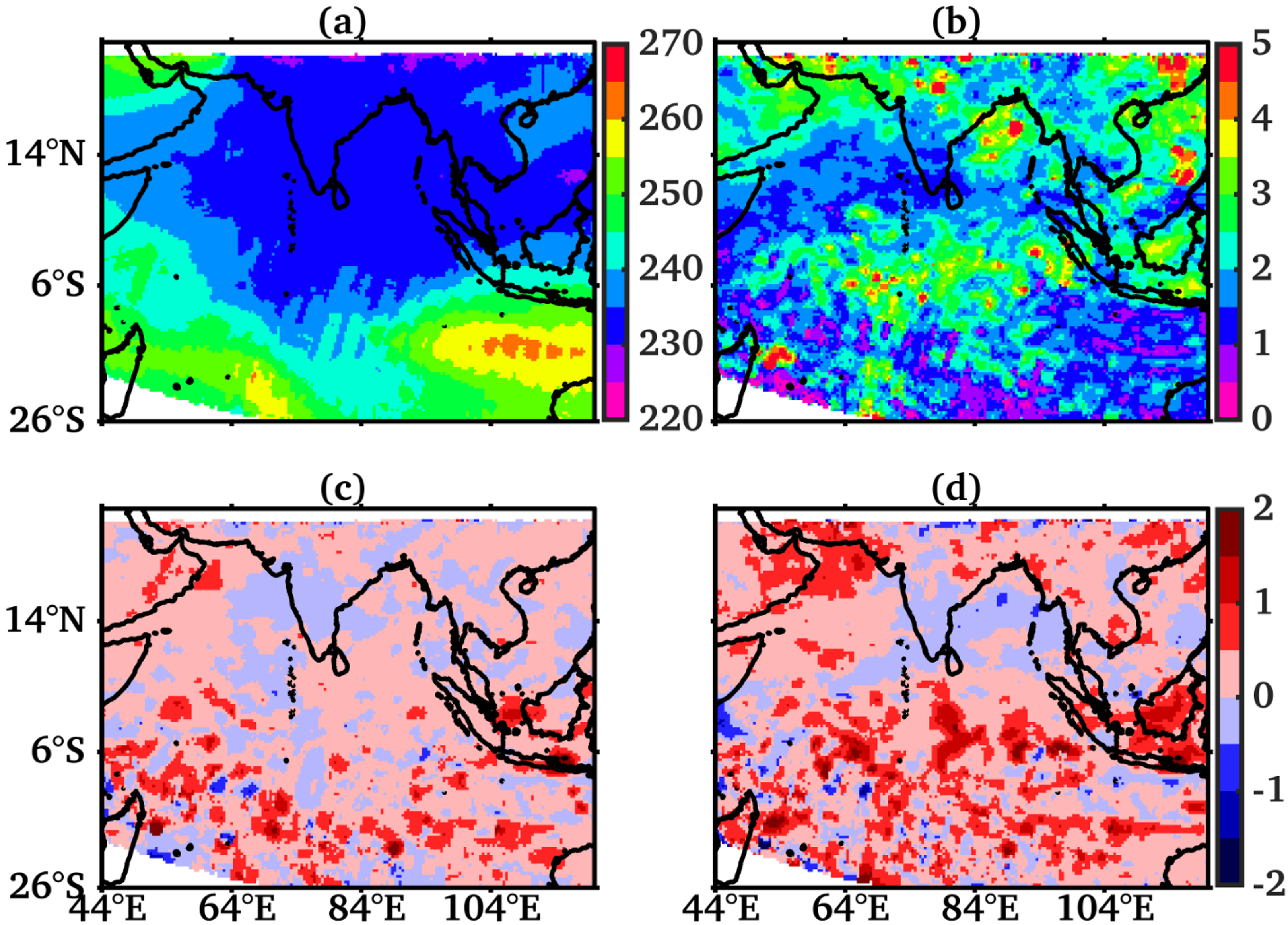

(a)
(b)
(c)
(d)
270
260
250
240
230
220
5
4
3
2
1
0
2
1
0
-1
-2
14°N
6°S
26°S
44°E
64°E
84°E
104°E

Figure 06.

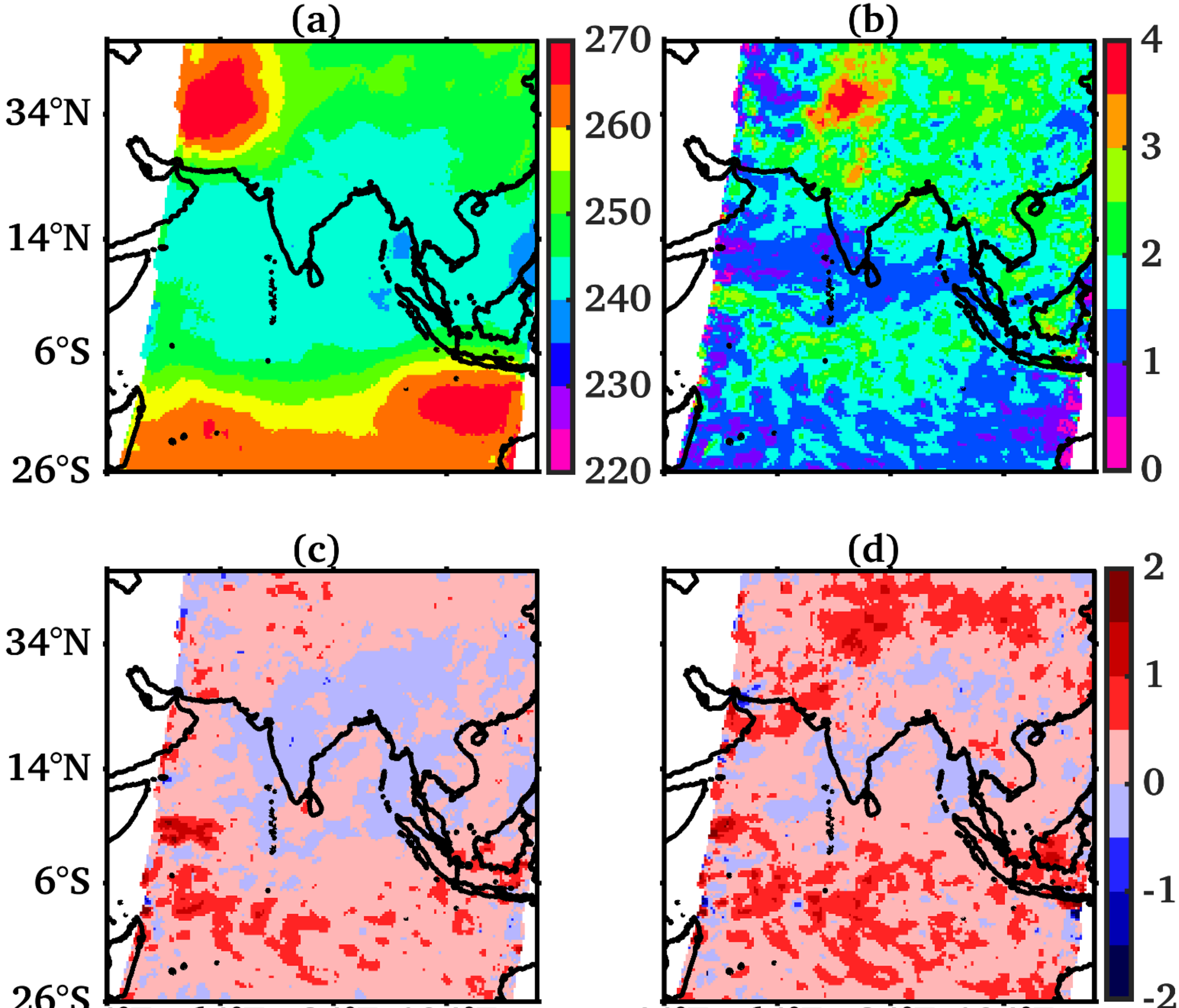
(a)
(b)
(c)
(d)
34°N
14°N
6°S
26°S
44°E
64°E
84°E
104°E
270
260
250
240
230
220
4
3
2
1
0
2
1
0
-1
-2

Figure 07.

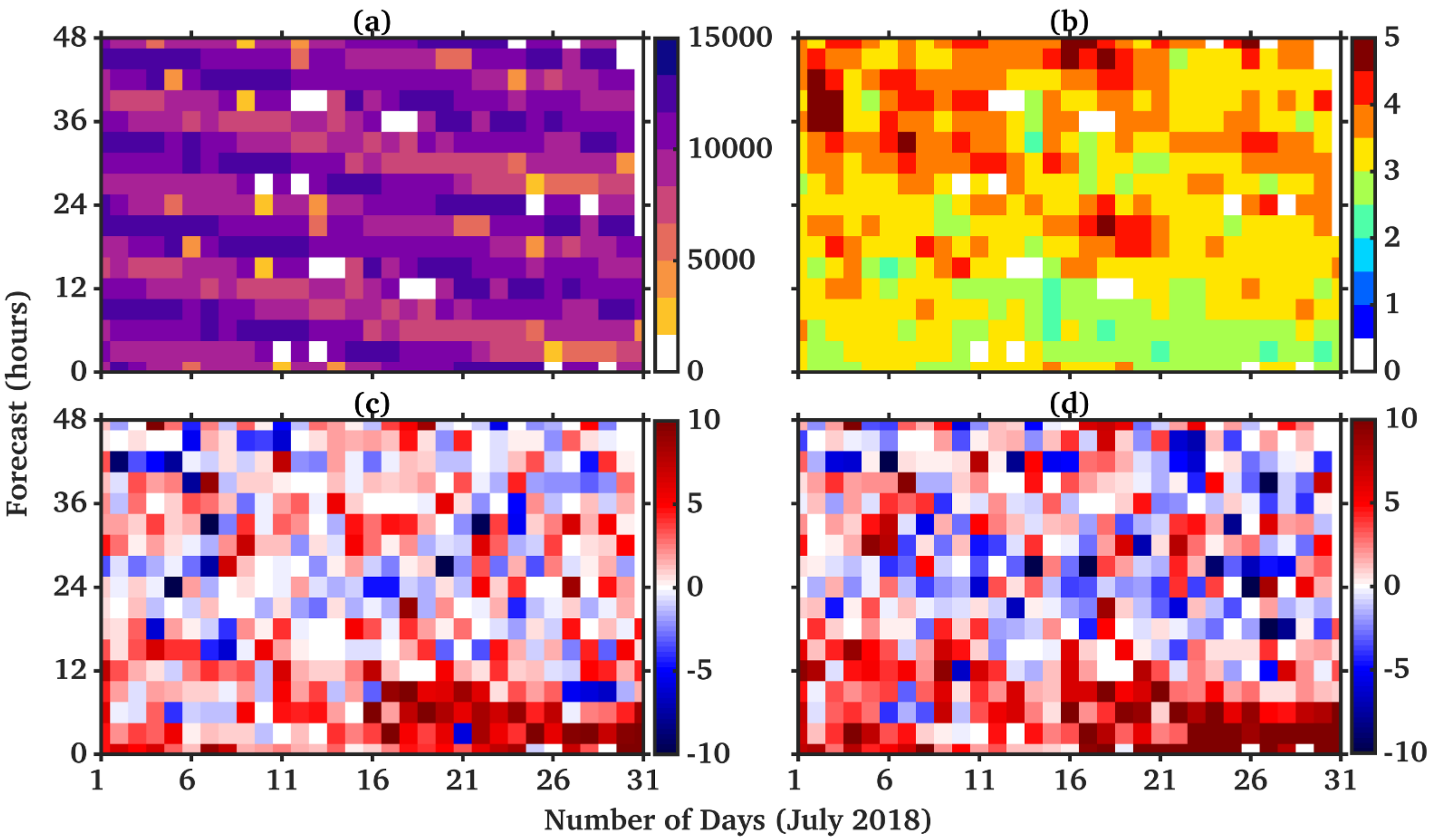

(a)
(b)
(c)
(d)
Forecast (hours)
Number of Days (July 2018)

Figure 08.

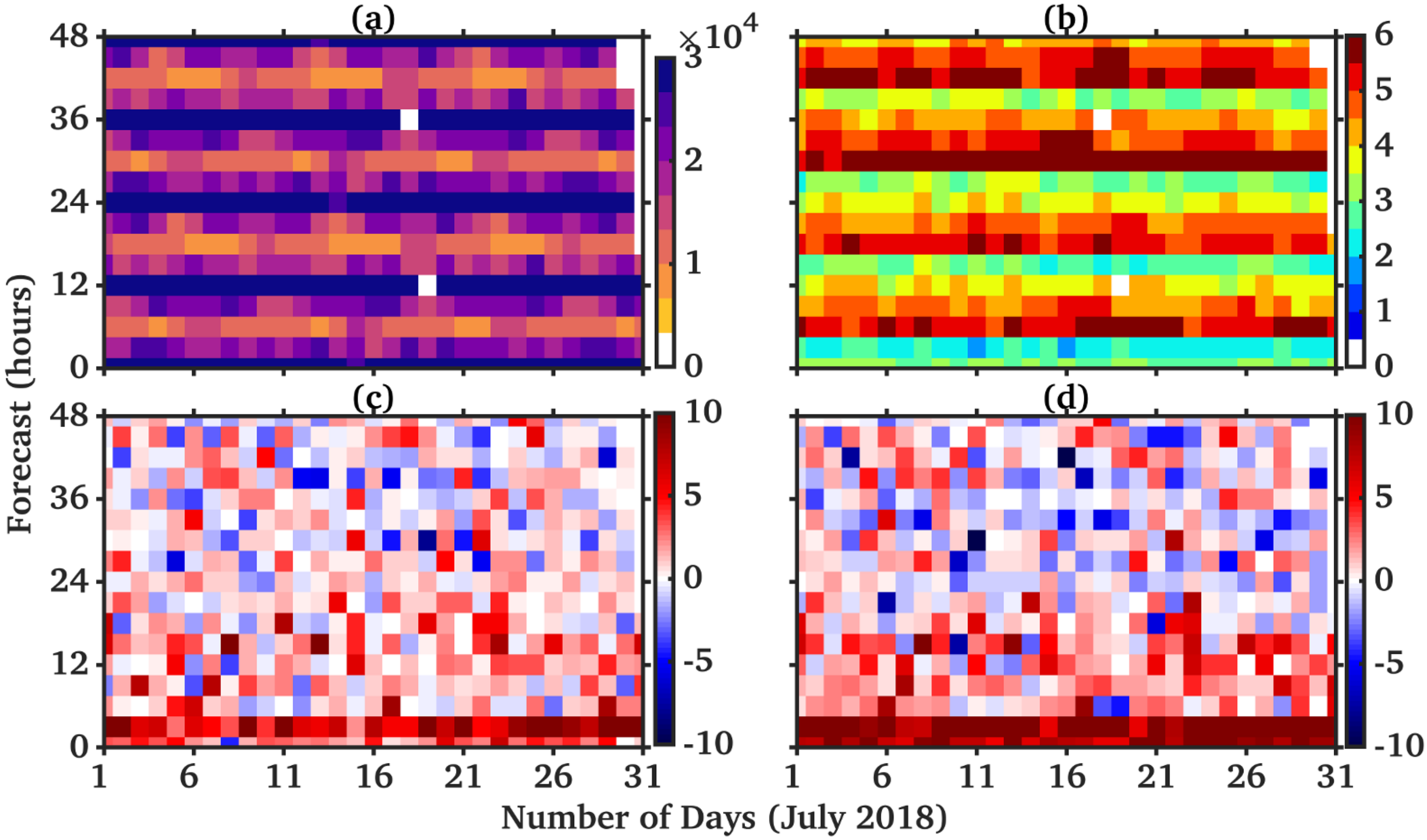

(a)
(b)
(c)
(d)
×10^4
Forecast (hours)
Number of Days (July 2018)

Figure 09.

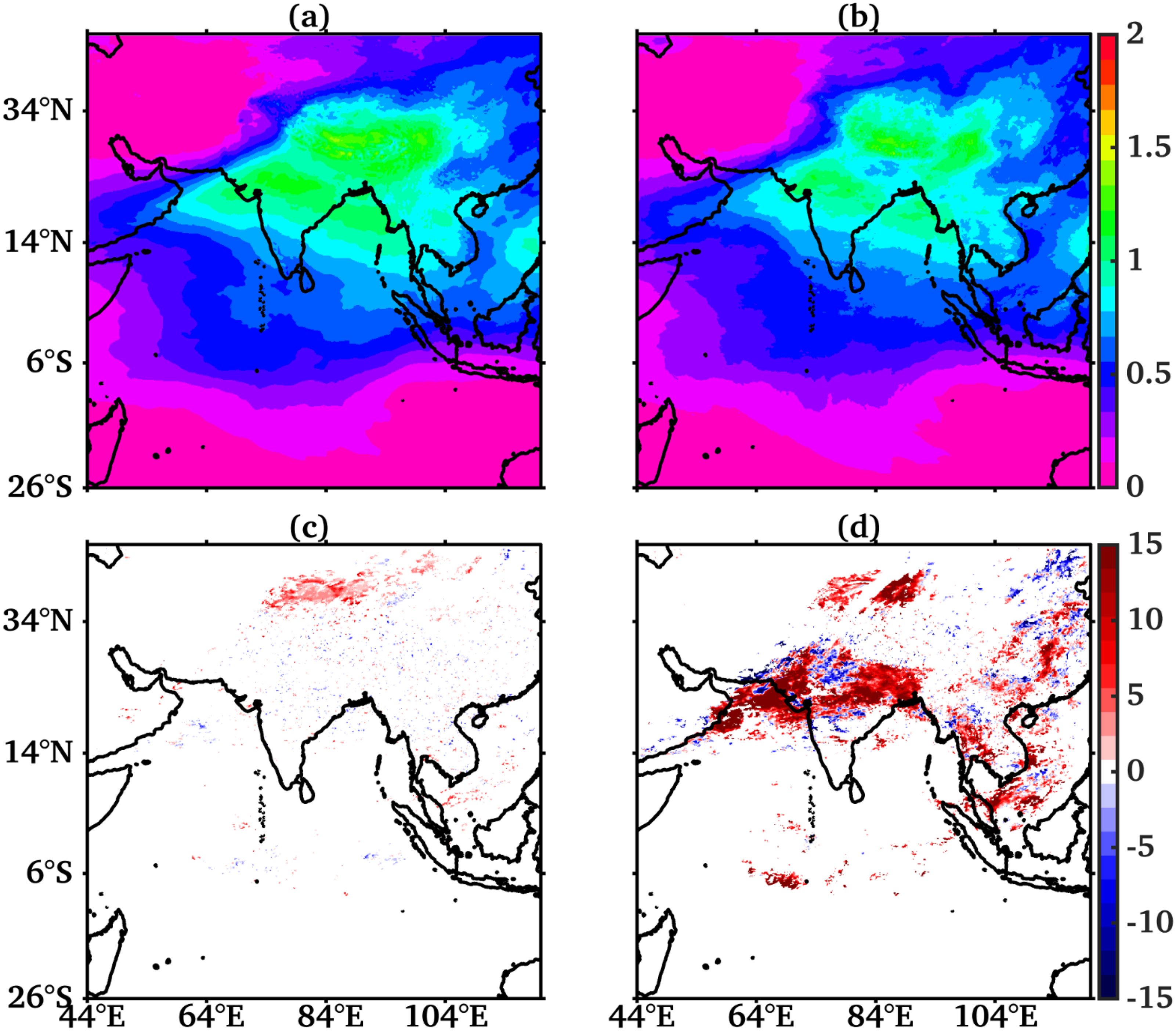
(a)
(b)
(c)
(d)
34°N
14°N
6°S
26°S
44°E
64°E
84°E
104°E
2
1.5
1
0.5
0
15
10
5
0
-5
-10
-15

Figure 10.

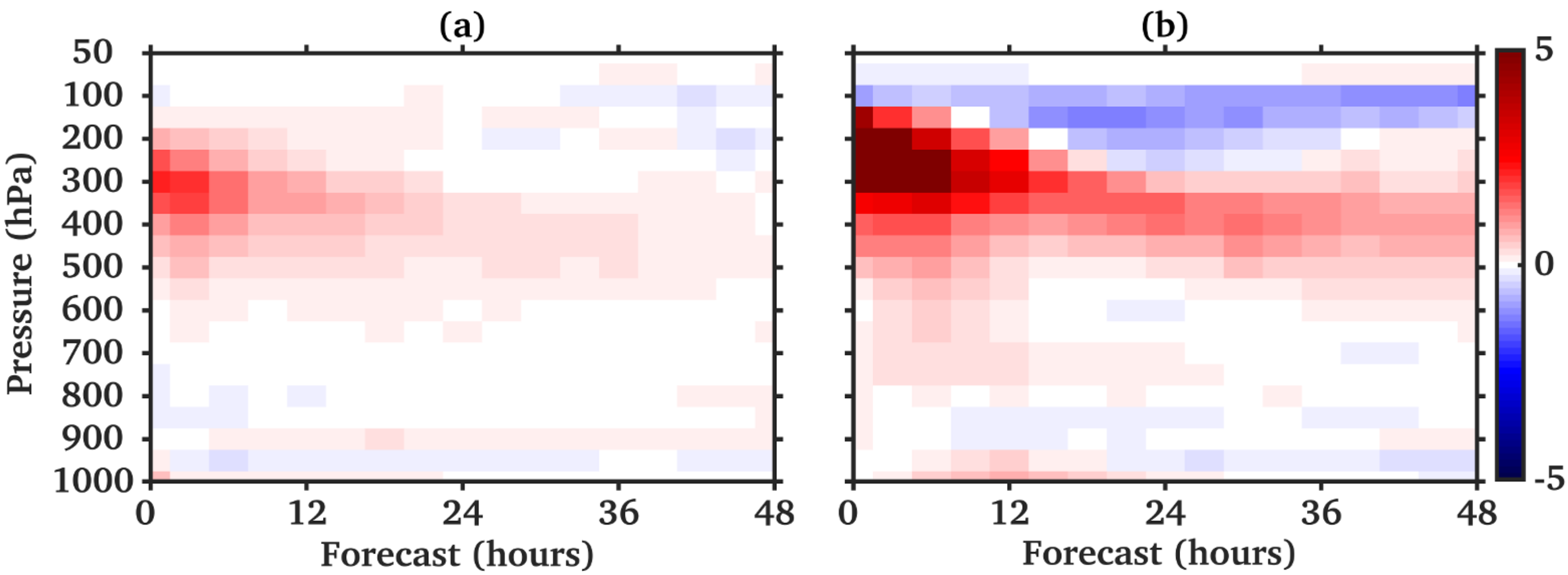

(a)
(b)
Pressure (hPa)
50
100
200
300
400
500
600
700
800
900
1000
0
12
24
36
48
Forecast (hours)
5
0
-5